CrossMark

Microwave absorption characteristics of Co^{2+} and W^{4+} substituted M-type $Ba_{0.5}Sr_{0.5}Co_xW_xFe_{12-2x}O_{19}$ hexagonal ferrites

Rajat Joshi[1] · Charanjeet Singh[1,3] · Dalveer Kaur[4] · S. Bindra Narang[3] ·
Rajshree Jotania[5] · Jasbir Singh[2]

Abstract The Co^{2+} and W^{4+} ions substituted M-type hexagonal ferrites, with chemical compositional formula $Ba_{0.5}Sr_{0.5}Co_xW_xFe_{12-2x}O_{19}$ (x = 0.0, 0.2, 0.8 and 1.0), were synthesized by a standard ceramic method. The phase evolution of the compositions was characterized by using an X-ray diffraction. The microwave absorption of compositions has been investigated as a function of frequency, substitution and thickness from 8.2 to 12.4 GHz by an absorber testing device method. The microwave absorption has been evaluated using the standard model of quarter wavelength mechanism and an impedance matching mechanism. The microwave absorption is enhanced in x = 0.0 and 0.2, with former owes 97.0 % absorbed power at 11.22 GHz and 2.4 mm respectively. Compositions x = 0.0, 0.2 and 0.8 exhibit −10 dB absorption bandwidth of 500 MHz while x = 1.0 owes 330 and 340 MHz.

✉ Charanjeet Singh
 charanjeet2003@rediffmail.com

1 Department of Electronics and Communication Engineering, Rayat Bahra Institute of Engineering and Nanotechnology, Hoshiarpur, Punjab, India

2 Department of Electronics and Communication Engineering, Yadavindra College of Engineering, Punjabi University Guru Kashi Campus, Talwandi Sabo, Punjab, India

3 Department of Electronics Technology, Guru Nanak Dev University, Amritsar, Punjab, India

4 Department of Electronics and Communication Engineering, I.K.G. Punjab Technical University, Kapurthla, India

5 Department of Physics, University School of Sciences, Gujarat University, Navrangpura, Ahmedabad, Gujarat, India

1 Introduction

The proliferation in information technology sector, associated with circuits of electronic devices operating at micro and millimeter wave regime, has given rise to the wireless or electromagnetic pollution. This undesired severity renders electromagnetic interference (EMI) leading to the malfunctioning of devices comprising of electrical and electronic circuits. The electronic devices, particularly oscillators or processors operating at GHz, generate harmonics or stray electromagnetic radiation causing bit error in the data received by wireless receivers. Furthermore, when the width of copper tracks of printed circuit boards is near to the quarter wavelength of the passing high frequency GHz signal, these tracks starts working as an antenna and radiate spurious electromagnetic signal referred as EMI. The microwave absorbers or radar absorbing materials (RAM) are used to suppress or attenuate this EMI or stray electromagnetic reflection from military aircraft, tank, radar etc.

Ferrites are employed in anteena, gyromagnetic devices, RAM, channel filters, tuning slug, radio frequency coil, wideband transformers etc. [1–4]. Their performance in electromagnetic interference (EMI) suppression is better compared to the conventional dielectric counterparts owing to the good magnetic properties. M-type hexagonal ferrites are ferrimagnetic in nature and incorporated particularly as microwave absorber, and exhibit dielectric and magnetic losses, domain wall resonance and ferromagnetic resonance (FMR) associated with spin relaxation [4, 5]. They show high resistivity at microwave frequencies which is pertinent for reducing the unwanted eddy currents.

The number of investigators has reported the microwave absorption in materials: Guanglei Wu et al. reported various investigations on hollow Fe_2O_3 microboxes, hematite

dendrites/polyaniline nanocomposite, urchin-like ZnO hollow spheres, γ-Fe_2O_3@C nanorod-carbon sphere composite, Ni_2O_3 nanoparticles, α-Fe_2O_3, γ-Fe_2O_3 and Fe_3O_4 nanospheres, Co–Co_3O_4 hybrid hollow sphere etc. [6–16]. Ji et al. [17] investigated M-type $BaFe_{12-x}(Mn_{0.5}Ti_{0.5})_xO_{19}$ hexagonal ferrite with substitution of Mn–Ti ions prepared by a ceramic method and found that the substitution lead to the increase in reflection loss to −31 dB. Baniasadi et al. [18] studied M-type Zn–Ti doped M-type Strontium hexagonal ferrite and obtained reflection loss of −36.58 at the maximum doping level. Cheng et al. [19] reported microwave absorption study in Co–Zr doped M-type $BaCo_xZr_xFe_{12-2x}O_{19}$ hexagonal ferrite and concluded that resonance frequency and resonance frequency can be controlled with Co–Zr ions. Li et al. [20] synthesized Cu–Ti doped M-type $Ba(CuTi)_xFe_{12-2x}O_{19}$ hexagonal ferrite and the composition x = 0.75 displayed reflection loss of −37 dB at 16.7 GHz with matching thickness of 1.6 mm. Ali-Sharbati et al. [21] investigated Ho substituted M-type $PbCo_{0.5}Sn_{0.5}Ho_xFe_{11-x}O_{19}$ hexagonal ferrites and substitution increased reflection loss to −33 dB at 16.5 GHz and 1.8 mm thickness.

Alam et al. [22] discussed the increase in absorption with thickness of composition and substitution of Mg^{2+}, Mn^{2+}, Co^{2+} and Ti^{4+} ions in M-type Barium ferrite and observed reflection loss (RL) of −16.4 dB at 11.5 GHz and 2.5 mm. Bercoff et al. [23] reported absorption increment with doping of Yt ions in Ni–Zn spinel ferrite. Sadiq et al. [24] concluded with reflection loss of −24.84 dB at 10.1 GHz in Sm^{3+} and Mn^{2+} ion co-doped X-type hexagonal ferrite. Tho et al. [25] put forth the role of quarter wavelength mechanism and impedance matching mechanism in absorption followed by −36.7 dB RL at 3 mm thickness in $La_{1.5}Sr_{1.5}NiO_4$ ferrite. Yu et al. [26] discussed absorption in Mn^{2+} ions doped $BaMn_xCo_{1-x}TiFe_{10}O_{19}$ hexagonal ferrite at Ku-band and maximum observed RL was −30.5 dB in x = 0.6 at 2 mm thickness.

In present investigation, we report microwave absorption property of M-type $Ba_{0.5}Sr_{0.5}Co_xW_xFe_{12-2x}O_{19}$ (x = 0.0, 0.2, 0.8 and 1.0) hexagonal ferrites prepared by a standard ceramic technique and evaluate the absorption with underlying mechanism associated with the quarter wavelength mechanism and an impedance matching mechanism, which to the authors' best knowledge is not reported yet.

2 Experimental

M-type hexagonal ferrite with compositions $Ba_{0.5}Sr_{0.5}Co_xW_xFe_{12-2x}O_{19}$ (x = 0.0, 0.2, 0.8 and 1.0) were prepare by a standard ceramic method [27]. The stoichiometric amount of different chemical reagents of compositions was

grounded in an agate pestle and mortar in the distilled water for 8 h. The ground mixed powders were pre-sintered at 1000 °C for 10 h in an electric furnace and obtained powders were grounded again under the same conditions. The sieving of powders was carried out with sieves of mesh size 220 B.S.S. and powders were converted into pellets with a hydraulic press at a uniaxial pressure of 75 KN/m^2 and the final sintering of pellets was carried out at 1250 °C for 20 h. X-ray powder diffraction patterns were scanned using Philips X'pert diffractometer equipped with a graphite crystal monochromator and copper target = 1.54056 Å. The working conditions for the X-ray tube were 40 kV and 25 mA. The each X-ray scan was performed between 10° and 70°.

The microwave characteristics of $Ba_{0.5}Sr_{0.5}Co_xW_xFe_{12-2x}O_{19}$ ferriteswere studied as a function of substitution, frequency and thickness at X-band by Absorber Testing Device (ATD) method [28, 29]: Fig. 1 shows block diagram of the adopted method.

The microwave frequency synthesizer, HP Model 83751A, generates frequencies at X-band (8–12 GHz) in the rectangular slotted waveguide with inner dimensions length = 22.86 mm, breadth = 10.16 mm. The isolator allows the unattenuated microwave propagation in one direction and vice versa. The directional coupler carries with one primary input and two secondary output ports. The composition, with metal plate, was fitted at the secondary output port and the reflected signal from composition was measured by power meter connected to other secondary output port. The microwave power meter Tektronix-Model 3320, was used to measure the different microwave signals and S_{11} parameter was calculated from reflected power at port 1.

The reflection loss (RL) can be expressed using following relation:

$$RL\ (dB) = 20\ \log_{10}(|S_{11}|) \tag{1}$$

The reflection loss of −10 dB represents 90 % microwave absorbed power and the large reflection loss corresponds to more microwave absorption and vice versa.

The reflected power (%) was calculated as:

$$Reflected\ Power\ (\%) = (P_r/P_{rw}) \times 100 \tag{2}$$

where P_r was the reflected power from the composition backed by metal plate and P_{rw} was the reflected power from the metal plate without composition.

The absorbed power was calculated using the following relation:

$$Absorbed\ Power\ (\%) = 100 - Reflected\ Power\ (\%) \tag{3}$$

The selected thickness of the composition corresponding to the optimised microwave absorption are: x = 0.0 (2.4 mm), x = 0.2 (2.8 mm), x = 0.8 (2.9 mm), x = 1.0
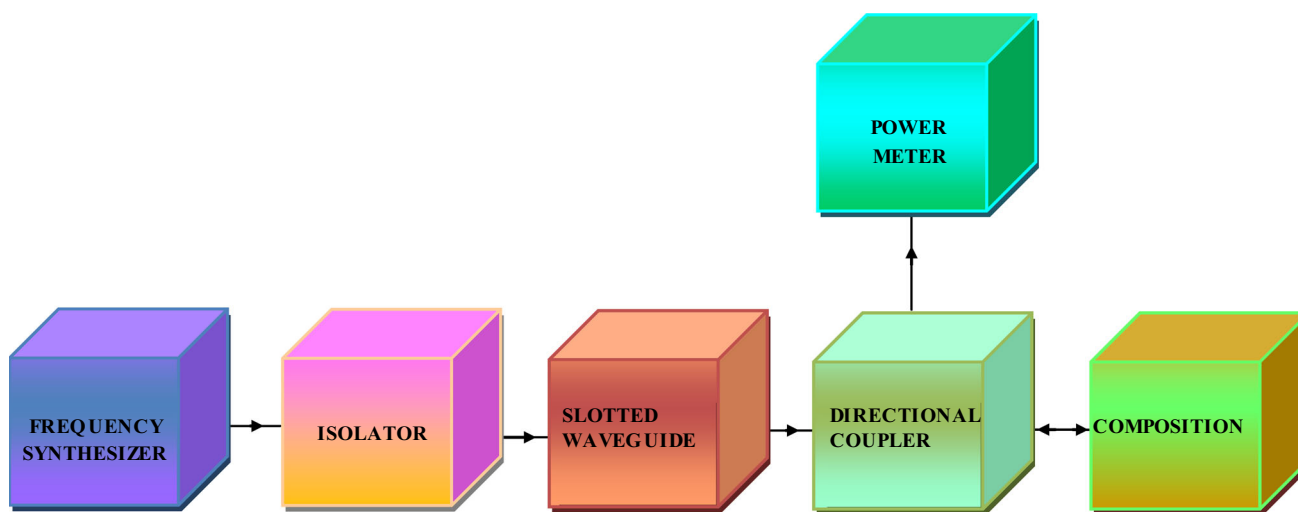
Fig. 1 Block diagram of ATD (absorber testing device) method

(2.5 mm). The term matching frequency (f_{mat}) and composition stands for the maximum power absorption at a particular frequency and composition.

3 Results and discussion

3.1 XRD analysis

The structural properties and phase purity of sintered compositions were investigated using X-ray diffraction technique. Figure 2a, b represents X-ray diffraction patterns of $Ba_{0.5}Sr_{0.5}Co_xW_xFe_{12-2x}O_{19}$ (x = 0.0, 0.2, 0.8 and 1.0) hexagonal ferrite compositions prepared using a standard ceramic method. All the observed peaks in XRD were identified with their Miller indices using MDI JADE and POWDER CELL software. The XRD patterns were indexed to hexagonal magnetoplumbite (M-type) crystal structure having space group P6$_3$/*mmc* (JCPDS file no. 51-1879).

The XRD analysis of x = 0.0 and 0.2 compositions confirms the formation of single M-type phase (hexagonal); while XRD analysis of x = 0.8 and 1.0 compositions revealed the formation of mixed crystalline phases of W (hexagonal, JCPDS file no. 19-0098), hematite-Fe_2O_3 (hexagonal, JCPDS file no 33-0664) and maghemite- γ-Fe_2O_3 (spinel, JCPDS file no. 39-1346). It seems that above for x > 0.2 composition, in the presence of Co^{2+} and W^{4+}, M-phase begins to decompose to Co_2W and W- phase formed. Since the sintered temperature of prepared compositions is low to form W-phase but tungsten oxides could help by acting as a flux. Neckenburger et al. [30, 31] found coexistence of different phases at the same temperature.

The lattice parameters (a = b and c) of compositions were calculated using following equation:

$$\frac{1}{d_{hkl}^2} = \frac{4}{3}\left(\frac{h^2}{a^2} + \frac{hk}{a^2} + \frac{k^2}{a^2}\right) + \frac{l^2}{c^2} \tag{4}$$

For hexagonal structure a = b $\neq$ c and $\alpha = \beta = 90°$ and $\gamma = 120°$, d_{hkl} as d-spacing of the lines in XRD pattern and h, k, l as Miller indices.

The variation of lattice parameters 'a' and 'c' as a function of Co–Al content (x) of all compositions is shown in Fig. 3. It is clear from the figure that lattice constant 'a' undergoes less variation compared to 'c' with the substitution of Co^{2+} and W^{4+} ions, which is a typical characteristic of hexagonal ferrites. The change in lattice parameters with the substitution may be due to the difference in ionic radii of Co (0.72 Å), W^{4+} (0.66 Å) and Fe (0.64 Å) [32, 33].

3.2 Reflection loss, microwave absorbed power

Figure 4 shows the variation of reflection loss (RL) as a function of frequency and substitution of Co^{2+} and W^{4+} ions in $Ba_{0.5}Sr_{0.5}Co_xW_xFe_{12-2x}O_{19}$ ferrites. The reflection loss increases at lower substitution of Co^{2+} and W^{4+} ions and all compositions exhibit RL more than −10 dB at low, middle and high frequency regime; compositions display highest RL (>−13 dB) at 11.22 GHz. The substitution of Co^{2+} and W^{4+} ions infers (1) change in amplitude of RL peaks (2) nearly no shift of RL peaks along the entire frequency region accompanied by the same peaks of maximal and minimal values almost at the same frequencies; large RL of −15.3 dB in x = 0.0 among all the compositions. The RL values are close in all compositions at most of the investigated frequencies.

Figure 5 exhibits the variation of absorbed power (P_{ab}) as a function of frequency and substitution of Co^{2+} and W^{4+} ions. Both lower and higher substituion observe large
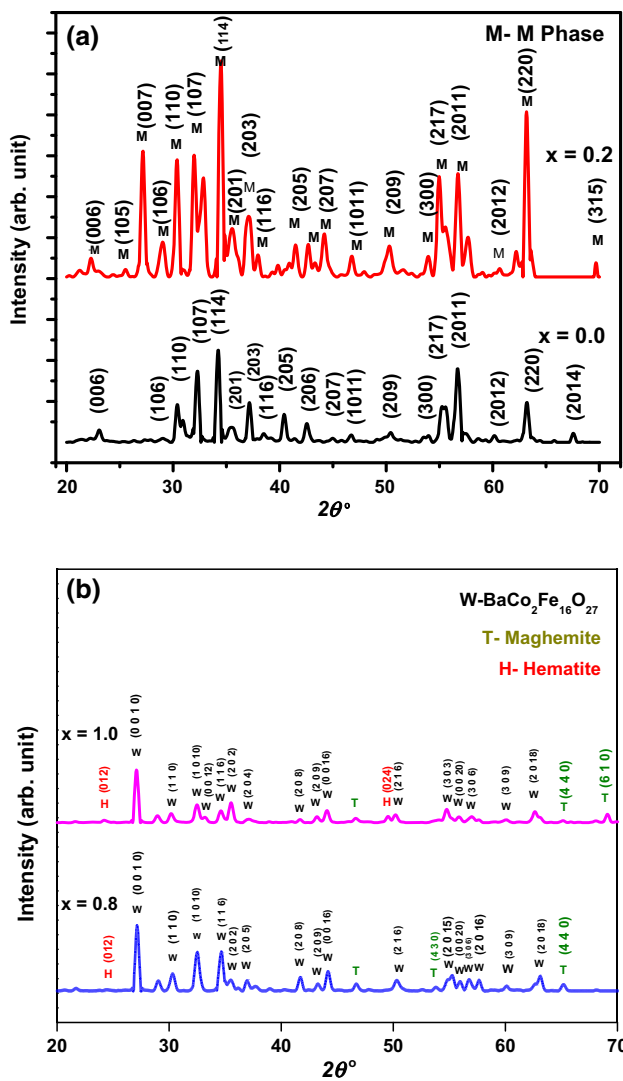
Fig. 2 a, b X-ray diffraction patterns of $Ba_{0.5}Sr_{0.5}Co_xW_xFe_{(12-2x)}O_{19}$ (x = 0.0, 0.2, 0.8 and 1.0) hexaferrite samples prepared using double sintering ceramic method and sintered at 1250 °C for 20 h
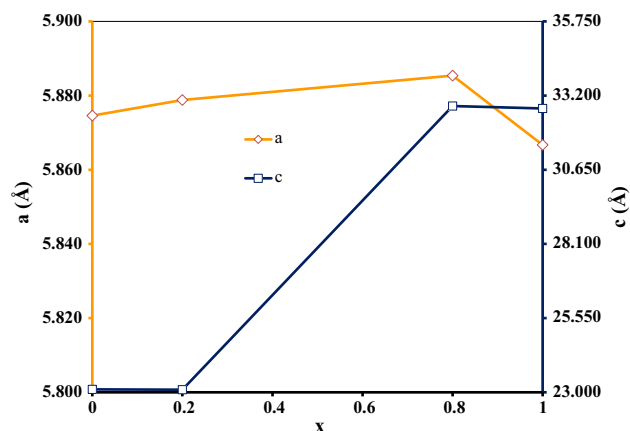

Fig. 3 The variation of lattice constants (*a*, *c*) and cell volume (*V*) with Co-W content of polycrystalline $Ba_{0.5}Sr_{0.5}Co_xW_xFe_{12-2x}O_{19}$ hexaferrite samples
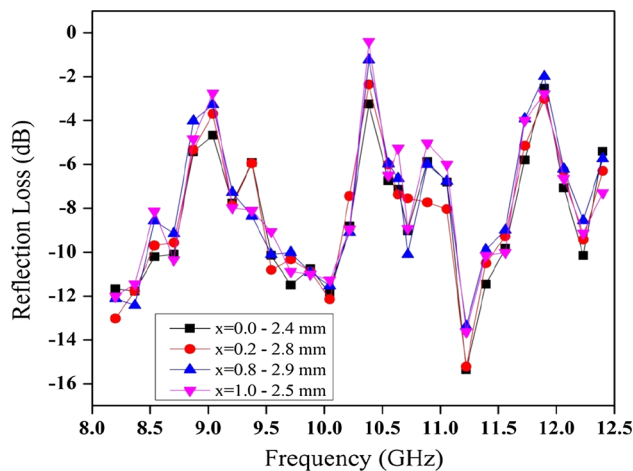
Fig. 4 Plots of reflection loss versus frequency and substitution in $Ba_{0.5}Sr_{0.5}Co_xW_xFe_{12-2x}O_{19}$ ferrites (x = 0.0, 0.2, 0.8 and 1.0)
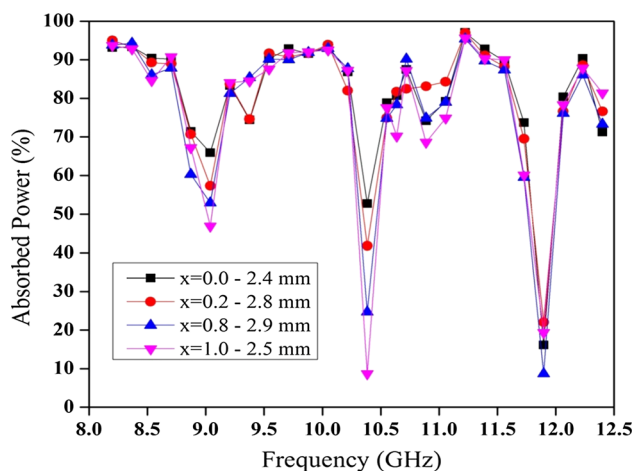
Fig. 5 Plots of absorbed power versus frequency and substitution in $Ba_{0.5}Sr_{0.5}Co_xW_xFe_{12-2x}O_{19}$ ferrites (x = 0.0, 0.2, 0.8 and 1.0)

P_{ab} along the investigated frequency region and more dispersion is seen from 10.38 to 11.05 GHz. The absorbed power is more than 90 % in all compositions along the different frequency regions. Composition x = 0.0 and 1.0 display highest and lowest P_{ab} of 97.7 and 9.2 % at 11.22 and 10.41 GHz respectively.

Table 1 shows maximum reflection loss (RL), maximum absorbed (P_{amax}), with corresponding matching frequency (f_{mat}), with the substituion of Co^{2+} and W^{4+} ions in $Ba_{0.5}Sr_{0.5}Co_xW_xFe_{12-2x}O_{19}$ ferrites. Composition x = 0.0 and x = 0.2 have comparatively more P_{amax} than x = 0.8 and 1.0. It increases with the substitution of Co^{2+} and W^{4+} ions. All compositions have P_{amax} at the same f_{mat} of 11.22 GHz followed by highest P_{amax} of 97.0 % in x = 0.0.

Table 1 Maximum reflection loss, maximum absorbed power, matching frequency, calculated or matching thickness, measured or experimental thickness, frequency band and bandwidth for RL > − 10 dB in $Ba_{0.5}Sr_{0.5}Co_xW_xFe_{12-2x}O_{19}$ ferrites (x = 0.0, 0.2, 0.8 and 1.0)

x	Reflection loss (dB)	P_{amax} (%)	Matching frequency (f_{mat}) (GHz)	Calculated thickness $t_m = \lambda/4$ (mm)	Measured thickness (t_{exp}) (mm) (experimental)	Frequency band RL > − 10 dB (GHz)	Bandwidth (MHz)
x = 0.0	−15.3	97.0	11.22	2.3	2.4	9.54–10.04	500
x = 0.2	−15.2	96.9	11.22	2.7	2.8	9.54–10.04	500
x = 0.8	−13.3	95.4	11.22	2.6	2.9	9.54–10.04	500
x = 1.0	−13.6	95.6	11.22	2.2	2.5	9.71–10.04	330
						11.22–11.56	340

3.3 Quarter wavelength mechanism

According to this mechanism [34, 35] when the thickness of ferrite absorber is equal to 1/4th wavelength of microwave signal, it will get attenuated or absorbed after passing through ferrite material.

When the microwave signal propagates through the ferrite composition backed by metal plate, a part of it will be partially reflected by the front surface of ferrite and the remaining signal will be transmitted through the ferrite. This transmitted signal gets reflected after reaching at the metal plate and arrives again at the front face of the ferrite. When the reflected signal from the front surface of ferrite composition is equal in magnitude and 180° out of phase with the reflected signal from the metal plate, both signals will cancel each other and total reflection will be zero. Therefore, this condition can be mathematically expressed as:

$$t_m = \frac{n\lambda_0}{4.\sqrt{\mu\varepsilon}} \qquad n = 1, 3, 5 \ldots \ldots \tag{5}$$

where t_m, λ_o, ε, and μ denote matching thickness, wavelength, complex permittivity, complex permeability and velocity of light respectively; Nicholson–Ross method [36] is used to derive ε and μ from S-parameters.

Table 1 depicts various parameters associated with the quarter wavelength mechanism applied to the compositions x = 0.0, 0.2, 0.8 and 1.0. The quarter wavelength mechanism is followed by x = 0.0, 0.2, 0.8 and 1.0 for the maximum absorption or RL peak in Figs. 3 and 4 at 11.22 GHz: the measured thickness of synthesized compositions is near to the theoretical thickness calculated using Eq. (5) of this mechanism (t = $\lambda_o/4$). Furthermore, Table 1 shows that RL or absorbed power is more in x = 0.0 and 0.2 as their measured thickness is more near to the theoretical thickness. However, RL is not much small in x = 0.8 and 1.0 in spite of the fact that their theoretical thickness is less close to measured thickness (Table 1) in comparison to x = 0.0 and 1.0. This anomaly is attributed

to the input impedance mechanism discussed in the next section.

Table 1 shows −10 dB bandwidth displayed by the compositions; −10 dB bandwidth means the band of frequencies for which RL is >−10 dB. Compositions x = 0.0, 0.2 and 0.8 exhibit 500 MHz absorption bandwidth (ABW) at the same frequency band from 9.54 to 10.04 GHz. Composition x = 1.0 has ABW of 330 MHz and 340 MHz from 9.71 to 10.04 GHz and 11.22–11.56 GHz respectively.

3.4 Impedance matching mechanism

The input impedance (Z_{in}) of a single layer absorber can be calculated theoretically on the basis of transmission line theory and can be expressed as [37]:

$$Z_{in} = Z_o(\mu/\varepsilon)^{1/2}tanh\left[j(2\pi ft/c)(\mu\varepsilon)^{1/2}\right] \tag{6}$$

where $Z_o = 377\ \Omega$ is the characteristic impedance of free space and t, f, ε, μ, c denote thickness, frequency, complex permittivity, complex permeability and velocity of light respectively.

When Z_{in} is equal to Z_o, input impedance of composition will be equal to characteristic impedance contributing infinite absorption of the signal by the composition.

The Eq. 6 explains that Z_{in} is of complex form (a + j b) where a is the real part and b is the imaginary part: (1) Theoretically all signal will be absorbed if $|Z| = Z_o = 377\Omega$, i.e. $Z_{real} = 377\ \Omega$ and $Z_{img} = 0$ (2) a component of signal RL will be absorbed when $Z_{real} \neq 377\ \Omega$ and/or $Z_{img} \neq 0$; when Z_{in} is equal or near to Z_o (377 Ω), it attributes to large microwave absorption due to impedance matching. Furthermore, absorption decreases when Z_{real} moves farther from 377 Ω and/or Z_{img} increases (positive or negative values).

Table 2 summarizes Z_{in}, Z_{real} and Z_{img} values corresponding to the large microwave absorption or RL peaks observed in compositions. It is evident from Table 2 that composition x = 0.8 and 1.0 have relatively both Z_{real} and Z_{img} more close to 377 Ω and zero respectively than that of

Table 2 Impdeance matching mechanism with f, Z_{in}, Z_{real} and Z_{img} values corresponding to RL peaks in $Ba_{0.5}Sr_{0.5}Co_xW_xFe_{12-2x}O_{19}$ ferrites (x = 0.0, 0.2, 0.8 and 1.0)

f (GHz)	RL peak (dB)	Z_{in} (Ω)	Z_{real} (Ω)	Z_{img} (Ω)	RL peak (dB)	Z_{in} (Ω)	Z_{real} (Ω)	Z_{img} (Ω)
	x = 0.0				x = 0.2			
8.2	−11.6	56.1	49.1	27.2	−13.0	47.9	38.8	28.0
8.368	−11.7	56.4	49.2	27.5	−11.7	48.2	39.1	28.1
8.536	−10.1	56.7	49.3	27.9	−9.6	48.5	39.3	28.3
8.704	−10.0	57.0	49.5	28.3	−9.5	48.8	39.6	28.4
9.544	−10.1	58.9	50.7	29.9	−10.8	50.6	41.2	29.4
9.712	−11.4	59.3	51.1	30.2	−10.3	51.0	41.6	29.6
9.88	−10.7	59.7	51.4	30.4	−10.8	51.5	42.0	29.8
10.048	−11.8	60.2	51.7	30.7	−12.1	51.9	42.4	30.0
11.224	−15.3	63.2	54.4	32.2	−15.2	55.5	45.6	31.5
11.392	−11.4	63.7	54.8	32.4	−10.4	56.0	46.2	31.8
12.232	−10.1	65.9	56.9	33.2	−9.4	59.3	49.2	33.1
	x = 0.8				x = 1.0			
8.2	−12.1	45.5	37.5	25.7	−11.9	33.5	29.5	15.8
8.368	−12.4	45.6	37.7	25.7	−11.4	33.4	29.1	16.3
8.536	−8.5	45.8	37.9	25.7	−8.1	33.5	29.0	16.8
8.704	−9.1	45.9	38.0	25.8	−10.3	33.6	29.0	17.0
9.544	−10.0	46.8	39.0	25.8	−9.0	37.3	31.0	20.7
9.712	−10.0	47.0	39.3	25.8	−10.8	39.5	32.8	21.9
9.88	−10.9	47.2	39.5	25.9	−11.0	42.5	36.6	21.6
10.048	−11.5	47.4	39.7	25.9	−11.2	42.0	38.6	16.6
11.224	−13.3	49.1	41.7	25.9	−13.6	36.8	31.8	18.4
11.392	−9.8	49.4	42.0	26.0	−10.1	37.4	32.5	18.5
12.232	−8.5	50.9	43.8	26.0	−9.1	37.4	32.2	19.0

x = 0.0 and 0.2. Therefore, the anomaly observed in the quarter wavelength mechanism of x = 0.8 and 1.0 is associated with a more contribution of the input impedance mechanism than x = 0.0 and 0.2. Similarly for other frequencies, the compositions have either Z_{real} away from 377 Ω or Z_{img} away from zero, thereby RL is less than 11.22 GHz: for example x = 0.0 owes highest Z_{real} = 56.9 Ω which is more towards Z_o = 377 Ω than at other frequencies, however, Z_{img} = 33.2 Ω is more far away from Z_{img} = 0. Tho et al. [25] reported similar variation in $La_{1.5}Sr_{0.5}NiO_4$ ferrites.

3.5 Screenshot of microwave signal

The screenshots are taken to show the frequency, phase and amplitude of the signal while passing through different compositions. Figure 6 depicts the observation of input signal applied to the compositions and signal transmitted from the compositions. The cathode ray oscilloscope (CRO) is used to display these signals: different frequencies applied to composition x = 0.0, 0.2, 0.8 and 1.0 are 8.36, 9.88, 8.70 and 11.22 GHz respectively. These screenshots elucidate for only attenuation of the signal by all compositions and frequency as well as phase of signal

remain unchanged. Similar variation was also seen for other signal applied at other frequencies.

4 Conclusions

The Co^{2+} and W^{4+} ions substituted $Ba_{0.5}Sr_{0.5}Co_xW_xFe_{12-2x}O_{19}$ hexagonal ferrites have been succesfully synthesized. Composition x = 0.0 exhibits the good microwave absorber or EMI reduction characteristics with 97 % absorbed power at matching frequency and thickness of 11.22 GHz and 2.4 mm respectively. Compositions x = 0.0, 0.2 and 0.8 exhibit 500 MHz absorption bandwidth (ABW) while x = 1.0 has ABW of 330 and 340 MHz. For maximum observed microwave absorption, x = 0.8 and 1.0 (W-type ferrite) have contribution of quarter wavelength as well as impedance matching mechanism, whereas x = 0.0 and 0.2 (M-type ferrite) have more contribution for quarter wavelength mechanism. The quarter wavelength and impedance matching mechanism can be implemented to predict thickness and frequency for the maximum microwave absorption. The synthesized compositions depict the potential for microwave absorber applications after making their composites with rubber,
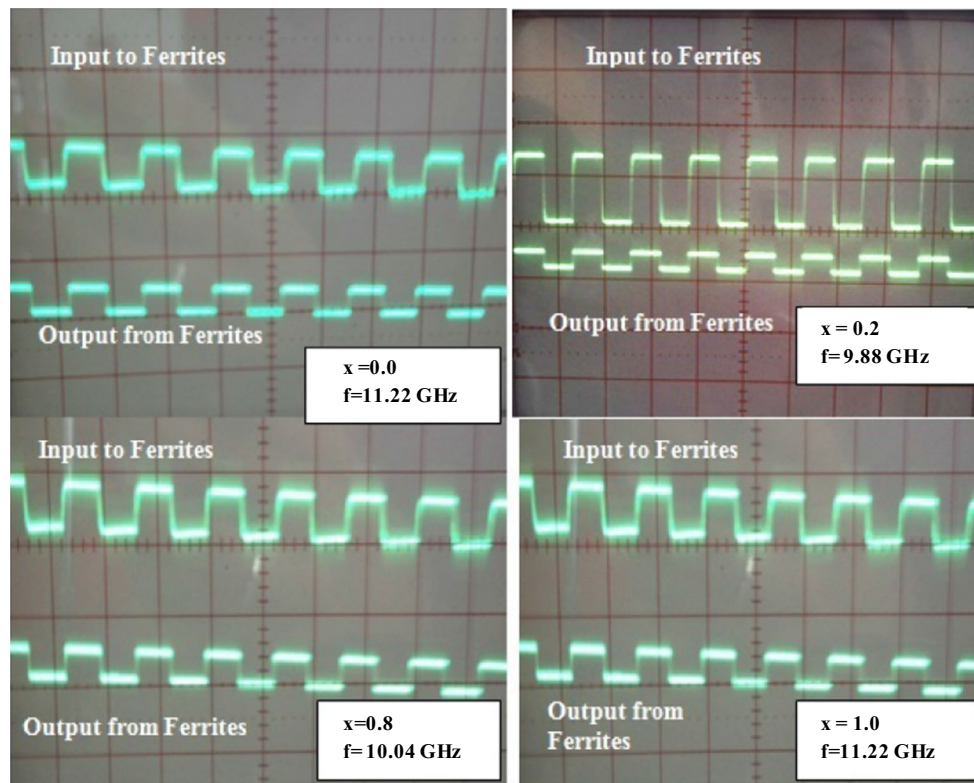
Fig. 6 Screenshot of input signal and signal transmitted through the compositions. (Amplitude value of signal is a guide to the eye)

polyaniline, wax etc., which is a topic of separate investigation.

References

1. J.C. Aphesteguy, A. Pamiani, D. Digiovanni, S.E. Jacobo, Microwave-absorbing characteristics of epoxy resin composites containing nanoparticles of NiZn and NiCuZn ferrites. Phys. B **404**, 2713 (2009)
2. X. Huang, J. Zhang, M. Lai, T. Sang, Preparation and microwave absorption mechanisms of the NiZn ferrite nanofibers. J. Alloys Compd. **627**, 367 (2015)
3. U.R. Lima, M.C. Nasar, M.C. Rezende, J.H. Araugo, Ni–Zn nanoferrite for radar-absorbing material. J. Magn. Magn. Mater. **320**, 1666 (2008)
4. P. Meng, K. Xiong, L. Wang, S. Li, Y. Cheng, G. Xu, Tunable complex permeability and enhanced microwave absorption properties of $BaNi_xCo_{1-x}TiFe_{10}O_{19}$. J. Alloys Compd. **628**, 75 (2015)
5. J. Liu, J. Zhang, P. Zhang, S. Wang, C. Lu, Y. Li, M. Zhang, Tunable microwave absorbing properties of barium hexa-ferrite nano powders by surface carbonized layers. Mater. Lett. **158**(53), 53–57 (2015)
6. H. Wu, G. Wu, Q. Wu, L. Wang, Facile synthesis and microwave absorbability of C@Ni–NiO core–shell hybrid solid sphere and multi-shelled NiO hollow sphere. Mater. Charact. **97**, 18 (2014)
7. H. Wu, G. Wu, L. Wang, Peculiar porous α-Fe_2O_3, γ-Fe_2O_3 and Fe_3O_4 nanospheres: facile synthesis and electromagnetic properties. Powder Technol. **269**, 443 (2015)
8. Y. Ren, L. Yang, L. Wang, T. Xu, G. Wu, H. Wu, Facile synthesis, photoluminescence properties and microwave absorption enhancement of porous and hollow ZnO. Powder Technol. **281**, 20 (2015)
9. H. Wu, Q. Wu, L. Wang, Design and wide range microwave absorption of porous Co–Co_3O_4 hybrid hollow sphere with magnetic multi-resonance mechanisms. Mater. Charact. **103**, 1 (2015)
10. W. Hu, L. Wang, Q. Wu, H. Wu, Facile synthesis, magnetic and optical properties of double-shelled Co_3O_4 hollow microspheres. Adv. Powder Technol. **25**, 1780 (2014)
11. H. Wu, G. Wu, Y. Ren, L. Yang, L. Wang, X. Lid, Co^{2+}/Co^{3+} ratio dependence of electromagnetic wave absorption in hierarchical $NiCo_2O_4$–$CoNiO_2$ hybrids. J. Mater. Chem. C **3**, 7677 (2015)
12. H. Wu, L. Wang, Y. Wang, S. Guo, Z. Shen, Enhanced microwave performance of highly ordered mesoporous carbon coated by Ni_2O3 nanoparticles. J. Alloys Compd. **525**, 82 (2012)
13. G. Wu, Y. Cheng, Y. Ren, Y. Wang, Z. Wang, H. Wu, Synthesis and characterization of γ-Fe_2O_3@C nanorod-carbon sphere composite and its application as microwave absorbing material. J. Alloys Compd. **652**, 346 (2015)
14. Q. Wu, G. Wu, L. Wang, W. Hu, H. Wu, Facile synthesis and optical properties of Prussian Blue microcubes and hollow Fe_2O_3 microboxes. Mater. Sci. Semicond. Process. **30**, 476 (2015)
15. H. Wu, L. Wang, H. Wu, Q. Lian, Synthesis and significantly enhanced microwave absorption properties of hematite dendrites/polyaniline nanocomposite. Appl. Phys. A **115**, 1299 (2014)
16. G. Wu, Y. Cheng, Q. Xie, Z. Jia, F. Xiang, H. Wu, Facile synthesis of urchin-like ZnO hollow spheres with enhanced electromagnetic wave absorption properties. Mater. Lett. **144**, 157 (2015)

17. K.-K. Ji, Y. Li, M.-S. Cao, Mn, Ti substituted barium ferrite to tune electromagnetic properties and enhanced microwave absorption. J. Mater. Sci.: Mater. Electron. **27**, 5128 (2016)

18. A. Baniasadi, A. Ghasemi, M.A. Ghadikolaei, A. Nemati, E. Paimozd, Microwave absorption properties of Ti–Zn substituted strontium hexaferrite. J. Mater. Sci.: Mater. Electron. **27**, 1901 (2016)

19. Y. Cheng, X. Ren, Permeability and electromagnetic wave absorption properties of sintered barium hexaferrites with substitution of Co^{2+}–Zr^{4+}. J. Mater. Sci.: Mater. Electron. **27**, 772 (2016)

20. S.S. Li, K. Xiong, P. Meng, X. Ren, G. Xu, Sol–gel synthesis of copper(II) and titanium(IV) ions co-doped barium ferrite submicrometer crystals and their microwave absorption performance. J. Mater. Sci.: Mater. Electron. **26**, 5710 (2015)

21. Ali-Sharbati, J.-M.V. Khani, Influence of Ho substitution on structural, magnetic and microwave absorption properties of PbM-type hexaferrites nanoparticles. J. Mater. Sci.: Mater. Electron. **25**, 244 (2014)

22. R.S. Alam, M. Moradi, H. Nikmanesh, J. Ventura, M. Rostami, Magnetic and microwave absorption properties of $BaMg_{x/2}Mn_{x/2}Co_xTi_{2x}Fe_{12-4x}O_{19}$ hexaferrite nanoparticles. J. Magn. Magn. Mater. **402**, 20 (2016)

23. S.E. Jacobo, P.G. Bercoff, Structural and electromagnetic properties of yttrium-substituted Ni–Zn ferrites range. Ceram. Int. **42**, 7664 (2016)

24. I. Sadiq, S. Naseem, M.N. Ashiq, M.A. Iqbal, I. Ali, M.A. Khan, S. Niaz, M.U. Rana, Spin canting effect and microwave absorption properties of Sm–Mn substituted nanosized material. J. Magn. Magn. Mater. **406**, 184 (2016)

25. P.T. Tho, C.T.A. Xuan, D.M. Quang, T.N. Bach, T.D. Thanh, N.T.H. Le, D.H. Manh, N.X. Phuc, D.N.H. Nam, Microwave absorption properties of dielectric $La_{1.5}Sr_{0.5}NiO_4$ ultrafine particles. Mater. Sci. Eng. **B186**, 101 (2014)

26. L. Wang, H. Yu, X. Ren, G. Xu, Magnetic and microwave absorption properties of $BaMn_xCo_{1-x}TiFe_{10}O_{19}$. J. Alloys Compd. **588**, 212 (2014)

27. C. Singh, S.B. Narang, I.S. Hudiara, Y. Bai, K. Marina, Hysteresis analysis of Co–Ti substituted M-type Ba–Sr hexagonal ferrite. Mater. Lett. **63**, 1991 (2009)

28. M.R. Meshram, N.K. Agrawal, B. Sinha, P.S. Misra, Characterization of M-type barium hexagonal ferrite-based wide band microwave absorber. J. Magn. Magn. Mater. **271**, 2007 (2004)

29. P. Singh, V.K. Babbar, A. Razdan, R.K. Puri, T.C. Goel, Complex permittivity, permeability, and X-band microwave absorption of CaCoTi ferrite composites. J. Appl. Phys. **87**, 4362 (2000)

30. E. Neckenburger, H. Severin, J.K. Vogel, G. Winkler, Ferrite hexagonaler Kristallstrustur mit hoher Grenzfrequenz. Z. Angew. Phys. **18**, 65 (1964)

31. R.C. Pullar, Hexagonal ferrites: a review of the synthesis, properties and applications of hexaferrite ceramics. Prog. Mater Sci. **57**, 1191 (2012)

32. C. Singh, S.B. Narang, I.S. Hudiara, Y. Bai, F. Tabatabaei, Static magnetic properties of Co and Ru substituted Ba–Sr ferrite. Mater. Res. Bull. **43**, 176 (2008)

33. C.B. Carter, M.G. Norton, *Ceramic materials: science and engineering* (Springer, Berlin, 2013), p. 58

34. B. Wang, J. Wei, Y. Yang, T. Wang, F. Li, Investigation on peak frequency of the microwave absorption for carbonyl iron/epoxy resin composite. J. Magn. Magn. Mater. **323**, 1101 (2011)

35. N.-N. Song, Y.J. Ke, H.-T. Yang, H. Zhang, X.-Q. Zhang, B.-G. Shen, Z.-H. Cheng, Integrating giant microwave absorption with magnetic refrigeration in one multifunctional intermetallic compound of $LaFe_{11.6}Si_{1.4}C_{0.2}H_{1.7}$. Sci. Rep. **2291**, 1 (2013)

36. A.M. Nicolson, G.F. Ross, Measurement of the intrinsic properties of materials by time-domain techniques. IEEE Trans. Instrum. Meas. **19**, 377 (1970)

37. T. Inui, K. Konishi, K. Oda, Fabrications of broad-band RF-absorber composed of planar hexagonal ferrites. IEEE Trans. Magn. **35**, 3148 (1999)